## 九州大学学術情報リポジトリ Kyushu University Institutional Repository

Domain switching dynamics in relaxor ferroelectric Pb(Mg\_<1/3>Nb\_<2/3>)0\_3-PbTi0\_3 revealed by time-resolved high-voltage electron microscopy

Sato, Kazuhisa Research Center for Ultra-High Voltage Electron Microscopy, Osaka University

Asakura, Naoya Research Center for Ultra-High Voltage Electron Microscopy, Osaka University

https://hdl.handle.net/2324/7393034

出版情報: Journal of Applied Physics. 130 (16), pp.164101-, 2021-10-26. AIP Publishing バージョン:

権利関係: This article may be downloaded for personal use only. Any other use requires prior permission of the author and AIP Publishing. This article appeared in Kazuhisa Sato, Naoya Asakura; Domain switching dynamics in relaxor ferroelectric Pb(Mg\_<1/3>Nb\_<2/3>)0\_3-PbTi0\_3 revealed by time-resolved high-voltage electron microscopy. J. Appl. Phys. 28 October 2021; 130 (16): 164101 and may be found at https://doi.org/10.1063/5.0064291.



# Domain switching dynamics in relaxor ferroelectric $Pb(Mg_{1/3}Nb_{2/3})O_3-PbTiO_3$ revealed by time-resolved high-voltage electron microscopy

Cite as: J. Appl. Phys. **130**, 164101 (2021); https://doi.org/10.1063/5.0064291 Submitted: 22 July 2021 • Accepted: 05 October 2021 • Published Online: 26 October 2021

🗓 Kazuhisa Sato and Naoya Asakura







### ARTICLES YOU MAY BE INTERESTED IN

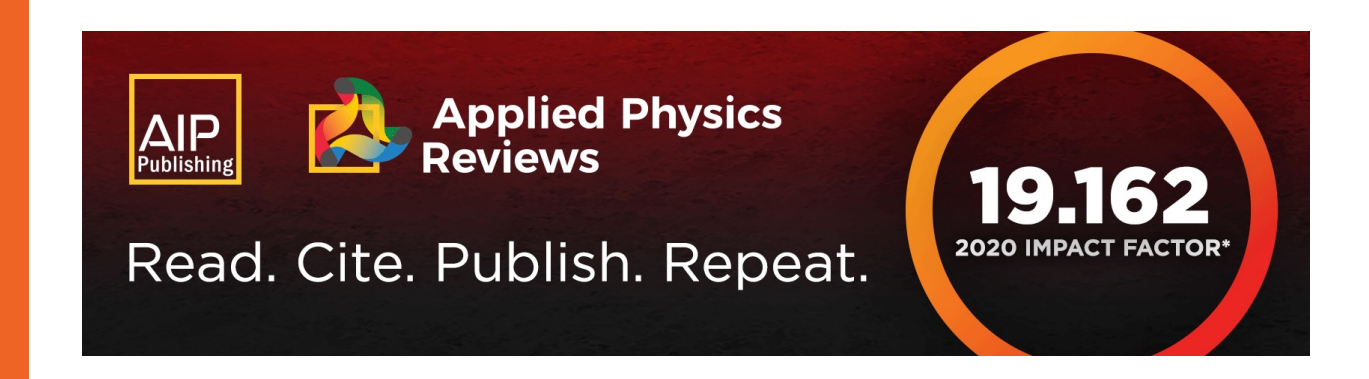
Perspective on photovoltaic optical power converters

Journal of Applied Physics 130, 160901 (2021); https://doi.org/10.1063/5.0070860

Modulating power delivery in a pulsed ICP discharge via the incorporation of negative feedback mechanisms

Journal of Applied Physics 130, 163304 (2021); https://doi.org/10.1063/5.0060240

Properties of higher-order surface acoustic wave modes in  $Al_{1-X}Sc_XN$ /sapphire structures Journal of Applied Physics 130, 164501 (2021); https://doi.org/10.1063/5.0055028





# Domain switching dynamics in relaxor ferroelectric Pb(Mg<sub>1/3</sub>Nb<sub>2/3</sub>)O<sub>3</sub>-PbTiO<sub>3</sub> revealed by time-resolved high-voltage electron microscopy

Cite as: J. Appl. Phys. 130, 164101 (2021); doi: 10.1063/5.0064291 Submitted: 22 July 2021 · Accepted: 5 October 2021 · Published Online: 26 October 2021







### **AFFILIATIONS**

Research Center for Ultra-High Voltage Electron Microscopy, Osaka University, 7-1 Mihogaoka, Ibaraki, Osaka 567-0047, Japan

a)Author to whom correspondence should be addressed: sato@uhvem.osaka-u.ac.jp

### **ABSTRACT**

Ferroelectric domain dynamics in Pb(Mg<sub>1/3</sub>Nb<sub>2/3</sub>)O<sub>3</sub>-0.3PbTiO<sub>3</sub> single crystals have been studied by in situ biasing high-voltage transmission electron microscopy with a direct electron detection camera. We have achieved time-resolved recording of polarization switching in real space on a 2.5 ms time scale. The reversible response of micrometer-scale domains was observed by applying an electric field of 1 kV/ mm. Detailed analyses on smaller sized domains 100-500 nm in size revealed that the domain switching initiated at a corner of a rectangular domain and propagated inward rapidly. The switching proceeded within 60 ms and the maximum switching rate, as fast as  $6-8 \mu m/s$ , was observed. The domain switching kinetics was classified as two-dimensional nucleation and growth mode based on the Kolmogolov-Avrami-Ishibashi model.

Published under an exclusive license by AIP Publishing. https://doi.org/10.1063/5.0064291

### I. INTRODUCTION

Ferroelectric materials such as Pb(Mg<sub>1/3</sub>Nb<sub>2/3</sub>)O<sub>3</sub>-PbTiO<sub>3</sub> (PMN-PT) are known as relaxor ferroelectrics characterized by excellent electromechanical properties that appear at the phase boundary (morphotropic phase boundary: MPB) between the rhombohedral and the tetragonal phases. 1-4 They have a wide range of potential applications such as ultrasonic probes, actuators, and capacitors. The relaxor ferroelectrics are characterized by inhomogeneous nanostructures known as polar nano-regions. To elucidate nanometer-scale ferroelectric domain configurations and their switching mechanism, in situ observation by transmission electron microscopy (TEM) is indispensable. Tan et al. reported the effect of a cyclic electric field on domain boundary cracking in a PMN-0.35PT single crystal.<sup>5,6</sup> Sato et al. revealed reversible response of polarization switching in a PMN-0.3PT single crystal by in situ TEM observations under electrical biasing.<sup>7,8</sup> Besides the PMN-PT, there are several examples of such in situ biasing observations on other ferroelectric materials, such as BiFeO<sub>3</sub> and Pb(Zr, Ti)O<sub>3</sub> (PZT) epitaxial films. 9-12 However, polarization switching on a nanometer-scale is usually so fast that aforementioned in situ imaging based on a conventional TV-rate [30 frames/s (fps)] charge-coupled device (CCD) camera can detect relatively slow dynamics. Newly developed direct electron detection (DED) cameras overcome this limit with frame rates of 400-1600 fps. 13-16 However, these high-performance cameras have not yet been used in the study of ferroelectrics.

An important point in TEM observation of the ferroelectric domain structures is the specimen thickness in electron propagation direction. Tsai and Cowley pointed out that domain width of BaTiO<sub>3</sub> films is thickness dependent due to surface relaxation effects.<sup>17</sup> Their experimental results clearly show reduction of the domain width as the thickness reduces in the thickness range of 20-80 nm. It should be noted that typical specimen thickness used for conventional 200 kV-class TEM observation is 10-100 nm. Therefore, a relatively thick TEM specimen is suitable for domain structure characterization. However, materials containing heavy element Pb (atomic number Z = 82) prevent clear-cut imaging due to strong electron scattering as the specimen thickness increases. To meet these rather conflicting demands, high-voltage transmission electron microscopy (HVEM) is a powerful tool in respect of maximum observable thickness with a high spatial resolution.<sup>1</sup> Alternative research methods include x-ray diffraction under electric fields<sup>20</sup> or piezoforce microscopy.<sup>21</sup> Although these advanced techniques have excellent advantages, it is practically impossible to

observe internal microstructures in real space. HVEM is hence the only technique that can reveal the ferroelectric domain structures of a relatively thick TEM foil with a high spatial resolution in a multiscale field of view up to tens of micrometer scale.

In this study, to elucidate domain switching dynamics in a thick PMN-PT single crystal, we employed *in situ* biasing HVEM using a DED CMOS camera. We developed an electrical biasing specimen holder for *in situ* HVEM observation compatible with high-angle specimen tilt of  $\pm 50^{\circ}$ . We have achieved time-resolved recording of domain switching in real space on a 2.5 ms time scale.

### II. EXPERIMENTAL PROCEDURE

TEM specimens of (1-x)Pb(Mg<sub>1/3</sub>Nb<sub>2/3</sub>)O<sub>3</sub>-xPbTiO<sub>3</sub> (PMN-xPT, nominal composition of x=0.3) single crystal were prepared in the following manner. First, a small piece of PMN-PT wafer approximately  $2\times2\times0.5$  mm<sup>3</sup> in size was glued on a molybdenum single hole TEM grid. Then, the crystal was thinned by mechanical polishing using a dimple grinder, followed by low-energy Ar ion milling at  $\sim$ 100 K, in order to ensure electron transparency. The thickness of the area used for HVEM observation was estimated to be 200–300 nm (Fig. S1 in the supplementary material). PT

content of  $x \sim 0.3$  was confirmed by TEM-EDS analysis (Table S1 in the supplementary material). The crystal structure of our specimens was regarded as monoclinic ( $M_{\rm B}$  phase, Cm) based on the compositional analysis together with the phase diagram<sup>4</sup> and crystal structure information reported in the literature. In the following, all indices are assigned based on the monoclinic ( $M_{\rm B}$ ) notation unless otherwise noted (a conversion relationship of Cm to pseudocubic is as follows:  $[100]_{Cm}//[110]_{cubic}$   $[001]_{Cm}//[001]_{cubic}$ .

In this study, we employed *in situ* biasing in a high-voltage electron microscope (JEOL JEM-1000EES installed at the Research Center for UHVEM, Osaka University) operating at 1 MV equipped with a DED CMOS camera (Gatan K2IS). We developed an electrical biasing specimen holder for *in situ* HVEM observation compatible with high-angle specimen tilt of  $\pm 50^{\circ}$ . The electrodes for *in situ* biasing experiments were fixed to the ion-milled specimen surface using silver paste. The electrodes were set across the perforation produced by ion milling. Spacing between the two electrodes was approximately 1 mm. The appearance of the electrodes is conceptually similar to that reported in the paper by Xu *et al.*<sup>6</sup> Electric fields up to  $1 \, \text{kV/mm}$  was applied in-plane to the specimen in a direction orthogonal to the longitudinal direction of the specimen holder using a dc power supply (see the supplemental material). The

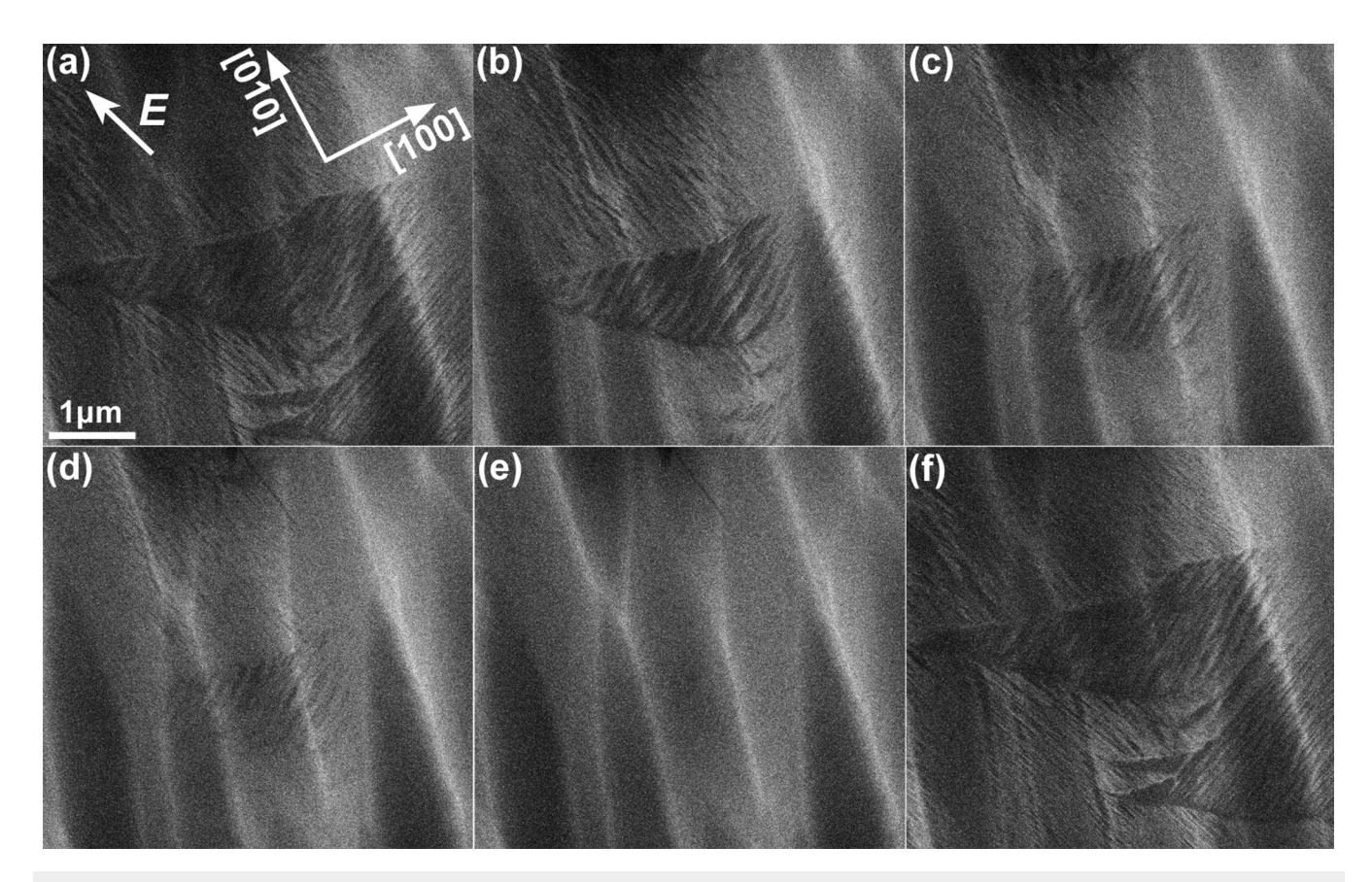


**FIG. 1.** BF-TEM images extracted from *in situ* biasing observation. The elapsed time after electric field application is as follows: (a) 0, (b) *t* = 440, (c) 690, (d) 815, (e) 1325, and (f) 19 625 ms (2310 ms after turning off the electric field).

electric field intensity was estimated by dividing an applied voltage by the distance between two electrodes. The DED CMOS camera enables fast image acquisition with a frame rate of 400 fps (2.5 ms/image). We set "look-back time" of the camera to be 1 s for image acquisition (Fig. S2 in the supplementary material). All the acquired images were processed using a dedicated software (Gatan GMS3).

### III. RESULTS

Figure 1 shows bright-field (BF) TEM images extracted from in situ biasing observation. The elapsed time after electric field application is as follows: (a) 0, (b) t = 440, (c) 690, (d) 815, (e) 1325, and (f) 19 625 ms (2310 ms after turning off the electric field). The image size is 1920 × 1792 pixels with the pixel size of 2.2 nm. The observation was performed at room temperature with electron flux of  $2 \times 10^{22}$  e/m<sup>2</sup>s. Under this observation condition, the effect of radiation damage due to the knock-on displacements on the domain structure is negligible (Table S2 in the supplementary material). The beam incident direction was in the [001] zone axis [indices were labeled assuming the monoclinic phase  $(M_{\rm B})$  with Cm symmetry  $^{22-25}$ ]. The polar axis of the monoclinic  $M_B$  phase lies in the ac mirror plane [(100) and (010)],<sup>23,25,26</sup> and hence the domain walls (DWs) are parallel to the {110} in the [001] projection. The specimen film was poled by applying electric field (E) of 1 kV/mm. The in-plane field direction was near [010] of the crystal (an arrow indicates the approximate direction of the electric field). In Fig. 1(a), ferroelectric domain structures of sub-micrometer to a few micrometers are seen. A low signal to noise ratio is inevitable for fast image acquisition (2.5 ms/image). In the triangular-shaped domain located at the center of the image, DWs are mostly parallel to  $(\bar{1}10)$  (i.e., projected DWs are in the [110] direction). These are considered to be the 90° a-a domains since the polar axis is in the ac planes [(100) and (010)]. Some of the DWs differ from neither {100} nor {110}. The DWs observed in the region surrounding the central triangular-shaped domain almost disappeared rapidly within 690 ms after the application of the electric field. In contrast, DWs in the central region was preserved until it disappeared at 1325 ms. These contrast variation in the DWs are due to rearrangement of domains in the electric field direction (movie S2 in the supplementary material). Once the electric field is turned off, domain contrast almost recovered after 2.3 s (movie S3 in the supplementary material). Such a reversible domain dynamics has also been reported in a previous study.7 It should be noted that crystal orientation slightly deviated when applying the electric fields, while the original excitation was almost retained (Fig. S3 in the supplementary material). Background stripes in the vertical direction are possibly due to surface morphology of the TEM specimen since they did not change with the electric field. A possible temperature rise due to in situ biasing can be negligible since there was no specimen drift during the observation.

Figure 2 shows details of domain switching process by *in situ* biasing obtained for another specimen. Domain sizes are  $\sim 100-500$  nm. In this field of view, the DWs are mostly parallel to  $\{110\}$ . These are considered to be  $90^{\circ}$  a-a domains. The elapsed time after electric field application is as follows: (a) 0 and (b) t=75 ms. The image size is  $1920 \times 1792$  pixels with the pixel size of 1.1 nm. The observation was made by exciting hh0 systematic

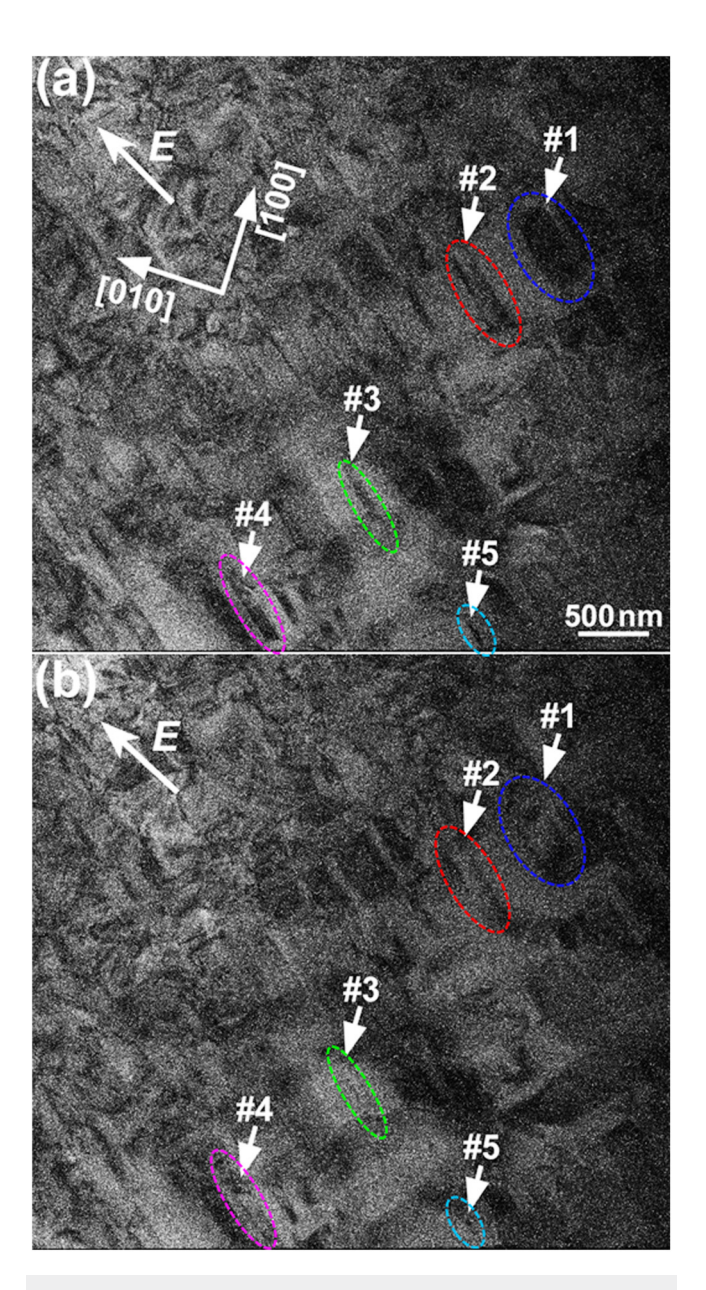


**FIG. 2.** BF-TEM images extracted from *in situ* biasing observation. The elapsed time after electric field application is as follows: (a) 0 and (b) t = 75 ms.

reflections. Electric field of 1 kV/mm was applied in a direction near [110] of the crystal (an arrow indicates the approximate direction of the electric field). After applying the electric field, BF-TEM images were taken every 2.5 ms (movie S1 in the supplementary material). In the following, we focused on five domains with different sizes as marked by arrows (#1–#5). In these domains, clear contrast changes were observed by applying the electric field. The change in domain contrast was then measured as a decrease in domain area.

Figure 3(a) shows degree of domain reversal (p) as a function of time after applying the electric field. The parameter p is defined as a value obtained by dividing an area of a reversed domain by its initial area. As seen, the domain reversal proceeded within  $\sim$ 60 ms, except for the domain #1, which had the largest initial area among the five domains investigated. The domain response showed a three-step process of (I) rearrangement start, (II) rapid movement, and (III) saturation. These fine structural changes could not be captured by a conventional TV-rate camera with time resolution of 33 ms and were first clarified in this study by utilizing DED CMOS camera. It was found that the maximum switching rates were in the range of 6–8  $\mu$ m/s and they were almost independent of the initial domain sizes as shown in Fig. 3(b). The obtained almost constant mobility may be arose from the polarization switching mechanism via nucleation and growth.

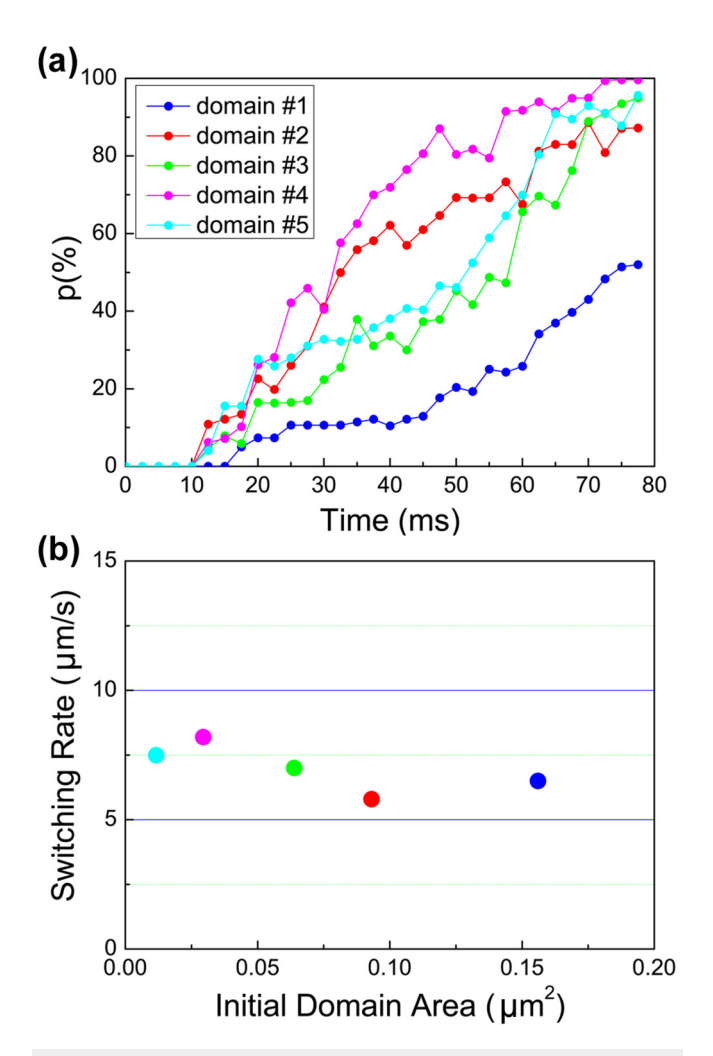


FIG. 3. (a) Degree of domain reversal (p) as a function of time after applying the electric field. (b) Maximum switching rates as a function of initial domain area.

Typical domain reversal process is shown in Fig. 4. A dark rectangular-shape contrast shows a ferroelectric domain. The scale bar corresponds to 100 nm. The electric field is in the longitudinal direction of the domain ( $E//\sim[110]$ ). In stage I, the morphological change begins slowly from the apex of the rectangular domain. Subsequently, in stage II, the morphological change rapidly progresses into the domain. In stage III, the contrast remains near the original DW, which eventually disappears.

### **IV. DISCUSSION**

We analyzed the results shown in Fig. 3 based on the Kolmogorov–Avrami–Ishibashi (KAI) model. This model represents a kinetics of solid-state phenomena via nucleation and growth. Degree of domain reversal (p) as a function of time can be expressed as follows:

$$p(t) = 1 - \exp\left[-\left(\frac{t}{t_0}\right)^n\right],\tag{1}$$

where n and  $t_0$  are the fitting parameters. Fitting curves for two extreme cases are shown in Fig. 5. The fit by the KAI model well reproduces the outline of the time dependence of the domain switching behavior. For the domains #2 and #1, n = 2.4 and 3.2 were obtained, respectively. Accordingly, all the obtained data show the n values between 2 and 3. According to the KAI model, nvalues of  $2 \le n \le 3$  indicate two-dimensional nucleation and growth mode. The *n* value for the domain #1 slightly exceeds 3 but this can be attributed to the fitting accuracy. As shown in Fig. 2(a), domains are rectangular-shape with sizes of  $\sim 100 \times \sim 500 \text{ nm}^2$ . On the other hand, specimen thickness is around 200-300 nm (Fig. S1 in the supplementary material). According to the literature, the non-ferroelectric layer due to surface relaxation is on the order of 10 nm in thickness, and hence possible structural artifact becomes apparent for a thin region less than ~50 nm. In this case, volume fraction of a non-ferroelectric artificial layer reaches as high as 40%, which may affect the domain structure characterization by TEM as a rough estimate. Thus, we emphasize here that the present study using HVEM excludes possible artifacts due to surface relaxation. Analytically derived two-dimensional nucleation and growth suggests that boundary between reversed and unreversed regions moves one-dimensionally in the electric field direction. This situation is emphasized when DWs are observed by TEM with edge-on condition (DWs are seen as a line) as employed in this study [Fig. 2(a)].

In respect of the crystal symmetry, the electric field direction significantly deviated from the polar axis [100] of the  $M_{\rm B}$  phase (Fig. 2), while the polarization reversal was observed. This result implies a possible coexistence of the monoclinic  $M_{\rm C}$  phase with Pm symmetry in our specimen. In this case, the polar axis exists on the (010) plane of the  $M_{\rm C}$  phase, which corresponds to the (110) plane of the  $M_{\rm B}$  phase (a conversion relationship of Cm to Pm is as follows:  $[100]_{Cm}//[110]_{Pm}$ ,  $[001]_{Cm}//[001]_{Pm}$ ).  $^{23,25,26}_{23,25,26}$  According to the x-ray study on PMN-xPT,  $^{22}_{10}$  the  $M_{\rm B}$  phase is stable in the composition range of  $0.27 \le x \le 0.30$ , while the  $M_{\rm C}$  phase is stable in  $0.31 \le x \le 0.34$ . The composition of our specimen (x = 0.3) is

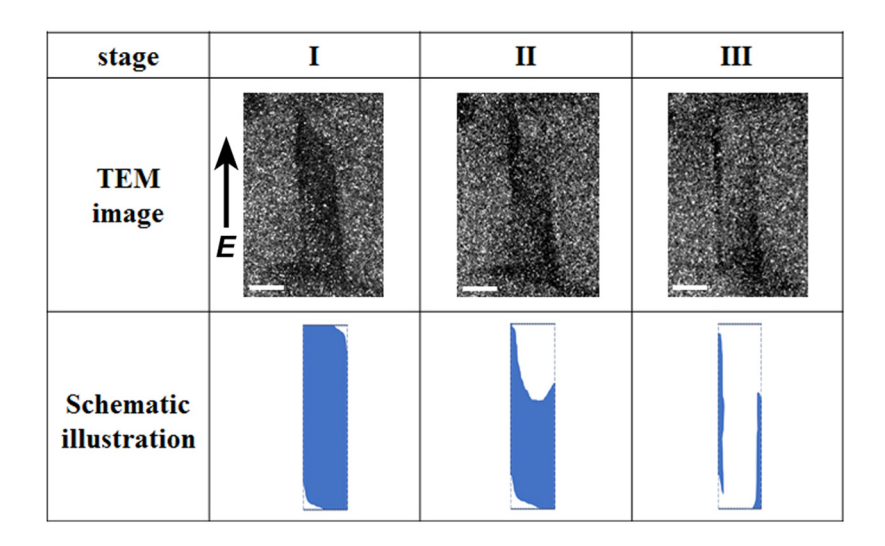


**FIG. 4.** Typical domain reversal process extracted from *in situ* biasing observation. The scale bar is 100 nm.

close to the phase boundary, and so it is plausible that the  $M_{\rm C}$  phase locally coexists, which facilitated the polarization switching.

Lam et al. reported the hysteresis loops of the PMN-0.35PT single crystal.<sup>30</sup> In their study, the single crystal was poled under the electric field of 1 kV/mm and the hysteresis loops showed coercive field of 0.58 kV/mm. Luo et al. also reported similar hysteresis loops for PMN-0.28PT single crystals.<sup>31</sup> Therefore, electric field of 1 kV/mm is sufficient to induce polarization switching. Actually, our experiments revealed that domain reversal occurred within 60 ms after the electric field application (Fig. 3). We have clarified an elementary process of polarization switching in a PMN-PT captured on the 2.5 ms time scale; however, there is a gap in the scale between macroscopic polarization switching and microstructural

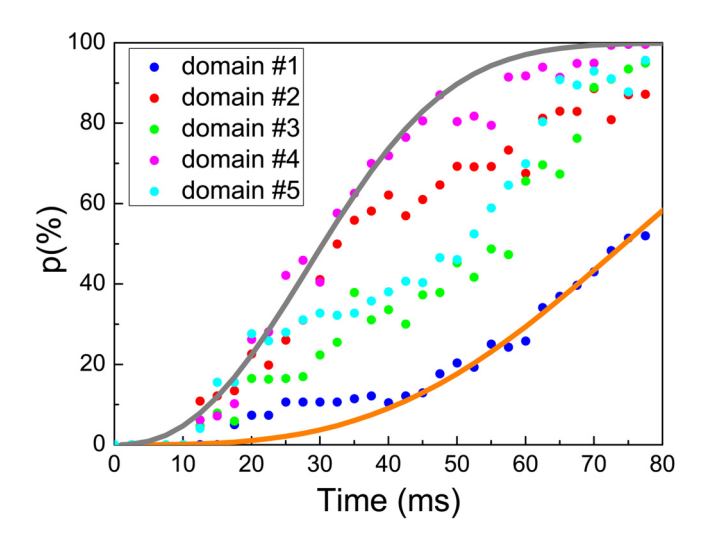


FIG. 5. Time dependence of the degree of domain reversal and their fitting based on the KAI model.

changes. Further study is needed to link multiscale results based on several experimental techniques in order to explain an excellent piezoelectricity of PMN-PT in terms of the elementary processes.

### V. CONCLUSIONS

In summary, the fast response of ferroelectric domains of PMN-PT single crystals has been studied by an in situ biasing using HVEM together with DED CMOS camera. We have achieved time-resolved recording of domain switching in real space on a 2.5 ms time scale. The switching proceeded within 60 ms, and the maximum switching rate, as fast as  $6-8 \mu m/s$ , was observed. Such a direct observation with a DED camera resulted in a breakthrough in temporal resolution over a conventional CCD camera. The domain switching kinetics was classified as two-dimensional nucleation and growth based on the KAI model ( $2.4 \le n \le 3.2$ ). In situ biasing HVEM combined with a DED CMOS camera is a powerful technique to reveal ferroelectric domain switching in thick ferroelectric materials. To detect the atomic process of polarization switching, another experimental setup with a nanosecond scale temporal resolution, such as pulse-TEM using a laser photocathode or a pump-probe technique, will be necessary.

### SUPPLEMENTARY MATERIAL

See the supplementary material for the detailed description of the experimental procedure and experimental conditions, together with movie files of *in situ* biasing observation.

### **ACKNOWLEDGMENTS**

The authors wish to thank Dr. H. Yasuda for invaluable comments and discussion. This study was partially supported by a Grant-in-Aid for Scientific Research (Grant Nos. 17H02746 and 19H02463) from the Ministry of Education, Culture, Sports, Science, and Technology, Japan.

### **AUTHOR DECLARATIONS**

### **Conflict of Interest**

The authors have no conflicts to disclose.

### DATA AVAILABILITY

The data that support the findings of this study are available within the article.

### **REFERENCES**

- S.-E. Park and T. R. Shrout, "Ultrahigh strain and piezoelectric behavior in relaxor based ferroelectric single crystals," J. Appl. Phys. 82, 1804–1811 (1997).
   B. Noheda, D. E. Cox, G. Shirane, J. A. Gonzalo, L. E. Cross, and S.-E. Park, "A monoclinic ferroelectric phase in the Pb(Zr<sub>1-x</sub>Ti<sub>x</sub>)O<sub>3</sub> solid solution," Appl. Phys. Lett. 74, 2059–2061 (1999).
- <sup>3</sup>H. Fu and R. E. Cohen, "Polarization rotation mechanism for ultrahigh electromechanical response in single-crystal piezoelectrics," Nature 403, 281–283 (2000).

  <sup>4</sup>B. Nodeda, D. E. Cox, G. Shirane, J. Gao, and Z.-G. Ye, "Phase diagram of the ferroelectric relaxor (1-x)Pb(Mg<sub>1/3</sub>Nb<sub>2/3</sub>)O<sub>3</sub>-xPbTiO<sub>3</sub>," Phys. Rev. B 66, 054104 (2002).

  <sup>5</sup>X. Tan, Z. Xu, J. K. Shang, and P. Han, "Direct observations of electric field-induced domain boundary cracking in <001> oriented piezoelectric Pb (Mg<sub>1/3</sub>Nb<sub>2/3</sub>)O<sub>3</sub>-PbTiO<sub>3</sub> single crystal," Appl. Phys. Lett. 77, 1529–1531 (2000).

  <sup>6</sup>Z. Xu, X. Tan, and J. K. Shang, "In situ transmission electron microscopy study of electric-field-induced microcracking in single crystal Pb(Mg<sub>1/3</sub>Nb<sub>2/3</sub>)
- O<sub>3</sub>-PbTiO<sub>3</sub>," Appl. Phys. Lett. **76**, 3732–3734 (2000).

  <sup>7</sup>Y. Sato, T. Hirayama, and Y. Ikuhara, "Real-time direct observations of polarization reversal in a piezoelectric crystal: Pb(Mg<sub>1/3</sub>Nb<sub>2/3</sub>)O<sub>3</sub>-PbTiO<sub>3</sub> studied via *in situ* electrical biasing transmission electron microscopy," Phys. Rev. Lett. **107**, 187601 (2011).
- <sup>8</sup>Y. Sato, T. Hirayama, and Y. Ikuhara, "Evolution of nanodomains under dc electrical bias in Pb(Mg<sub>1/3</sub>Nb<sub>2/3</sub>)O<sub>3</sub>-PbTiO<sub>3</sub>: An *in situ* transmission electron microscopy study," Appl. Phys. Lett. **100**, 172902 (2012).
- <sup>9</sup>C. T. Nelson, P. Gao, J. R. Jokisaari, C. Heikes, C. Adamo, A. Melville, S.-H. Baek, C. M. Folkman, B. Winchester, Y. Gu, Y. Liu, K. Zhang, E. Wang, J. Li, L.-Q. Chen, C.-B. Eom, D. G. Schlom, and X. Pan, "Domain dynamics during ferroelectric switching," Science 334, 968–971 (2011).
- <sup>10</sup>P. Gao, C. T. Nelson, J. R. Jokisaari, S.-H. Baek, C. W. Bark, Y. Zhang, E. Wang, D. G. Schlom, C.-B. Eom, and X. Pan, "Revealing the role of defects in ferroelectric switching with atomic resolution," Nature Commun. 2, 591 (2011).
- <sup>11</sup>P. Gao, J. Britson, C. T. Nelson, J. R. Jokisaari, C. Duan, M. Trassin, S.-H. Baek, H. Guo, L. Li, Y. Wang, Y.-H. Chu, A. M. Minor, C.-B. Eom, R. Ramesh, L.-Q. Chen, and X. Pan, "Ferroelastic domain switching dynamics under electrical and mechanical excitations," Nature Commun. 5, 3801 (2014).
- <sup>12</sup>J. K. Lee, G. Y. Shin, K. Song, W. S. Choi, Y. A. Shin, S. Y. Park, J. Britson, Y. Cao, L.-Q. Chen, H. N. Lee, and S. H. Oh, "Direct observation of asymmetric domain wall motion in a ferroelectric capacitor," Acta Mater. 61, 6765–6777 (2013).
  <sup>13</sup>H.-G. Liao, D. Zherebetskyy, H. Xin, C. Czarnik, P. Ercius, H. Elmlund, M. Pan, L.-W. Wang, and H. Zheng, "Facet development during platinum nanocube growth," Science 345, 916–919 (2014).

- <sup>14</sup>V. Migunov, H. Ryll, X. Zhuge, M. Simson, L. Strüder, K. J. Batenburg, L. Houben, and R. Dunin-Borkowski, "Rapid low dose electron tomography using a direct electron detection camera," Sci. Rep. 5, 14516 (2015).
- <sup>15</sup>K. Sato and H. Yasuda, "Fluctuation of long-range order in Co-Pt alloy nanoparticles revealed by time-resolved electron microscopy," Appl. Phys. Lett. 110, 153101 (2017).
- <sup>16</sup>H. Yasuda, "Fast in situ ultrahigh-voltage electron microscopy observation of crystal nucleation and growth in amorphous antimony nanoparticles," Cryst. Growth Des. 18, 3302–3306 (2018).
- <sup>17</sup>F. Tsai and J. M. Cowley, "Thickness dependence of ferroelectric domains in thin crystalline films," Appl. Phys. Lett. 65, 1906–1908 (1994).
- <sup>18</sup>K. Sato and H. Yasuda, "Probing crystal dislocations in a micrometer-thick GaN film by modern high-voltage electron microscopy," ACS Omega 3, 13524–13529 (2018).
- <sup>19</sup>K. Sato and H. Yasuda, "Athermal crystal defect dynamics in Si revealed by cryo-high-voltage electron microscopy," ACS Omega 5, 1457–1462 (2020).
- 20°C. Moriyoshi, S. Hiramoto, H. Ohkubo, Y. Kuroiwa, H. Osawa, K. Sugimoto, S. Kimura, M. Takata, Y. Kitanaka, Y. Noguchi, and M. Miyayama, "Synchrotron radiation study on time-resolved tetragonal lattice strain of BaTiO<sub>3</sub> under electric field," Jpn. J. Appl. Phys. 50, 09NE05 (2011).
- <sup>21</sup>Y. Kutes, L. Ye, Y. Zhou, S. Pang, B. D. Huey, and N. P. Padture, "Direct observation of ferroelectric domains in solution-processed CH<sub>3</sub>NH<sub>3</sub>PbI<sub>3</sub> perovskite thin films," J. Phys. Chem. Lett. 5, 3335–3339 (2014).
- **22** A. K. Singh and D. Pandey, "Evidence for  $M_B$  and  $M_C$  phases in the morphotropic phase boundary region of  $(1-x)[Pb(Mg_{1/3}Nb_{2/3})O_3]-xPbTiO_3$ : A rietveld study," Phys. Rev. B **67**, 064102 (2003).
- $^{23}$ K.-H. Kim, D. A. Payne, and J.-M. Zuo, "Symmetry of piezoelectric (1-x)Pb  $(Mg_{1/3}Nb_{2/3})O_3$ -xPbTiO $_3$  (x=0.31) single crystal at different length scales in the morphotropic phase boundary region," Phys. Rev. B **86**, 184113 (2012).
- <sup>24</sup>D. Vanderbilt and M. H. Cohen, "Monoclinic and triclinic phases in higher-order Devonshire theory," Phys. Rev. B 63, 094108 (2001).
- <sup>25</sup>Z. Chen, Z. Luo, C. Huang, Y. Qi, P. Yang, L. You, C. Hu, T. Wu, J. Wang, C. Gao, T. Sritharan, and L. Chen, "Low-symmetry monoclinic phases and polarization rotation path mediated by epitaxial strain in multiferroic BiFeO<sub>3</sub> thin films," Adv. Funct. Mater. 21, 133–138 (2011).
- <sup>26</sup>B. Noheda, J. A. Gonzalo, L. E. Cross, R. Guo, S.-E. Park, D. E. Cox, and G. Shirane, "Tetragonal-to-monoclinic phase transition in a ferroelectric perovskite: The structure of PbZr<sub>0.52</sub>Ti<sub>0.48</sub>O<sub>3</sub>," Phys. Rev. B **61**, 8687 (2000).
- <sup>27</sup>Y. Ishibashi and Y. Takagi, "Note on ferroelectric domain switching," J. Phys. Soc. Jpn. 31, 506–510 (1971).
- <sup>28</sup>H. Orihara and Y. Ishibashi, "A statistical theory of nucleation and growth in finite systems," J. Phys. Soc. Jpn. 61, 1919–1925 (1992).
- 29 Y. Ivry, J. F. Scott, E. K. H. Salje, and C. Durkan, "Nucleation, growth, and control of ferroelectric-ferroelastic domains in thin polycrystalline films," Phys. Rev. B 86, 205428 (2012).
- <sup>30</sup>K. H. Lam, H. L. W. Chan, C. L. Choy, H. S. Luo, Q. R. Yin, and Z. W. Yin, "Properties of PMN-PT fibres fabricated using powder of PMN-PT single crystals," Ceram. Int. 30, 1939–1943 (2004).
- <sup>31</sup>L. Luo, M. Dietze, C.-H. Solterbeck, H. Luo, and M. Es-Souni, "Tuning the functional properties of PMN-PT single crystals via doping and thermoelectrical treatments," J. Appl. Phys. 114, 224112 (2013).